NMR and Modeling Studies of Protein–Carbohydrate Interactions: Synthesis, Three-Dimensional Structure, and Recognition Properties of a Minimum Hevein Domain with Binding Affinity for Chitooligosaccharides

Nuria Aboitiz,[a] Miquel Vila-Perelló,[b] Patrick Groves,[a] Juan Luis Asensio,[a] David Andreu,[b] Francisco Javier Cañada,*[a] and Jesús Jiménez-Barbero*[a]

HEV32, a 32-residue, truncated hevein lacking eleven C-terminal amino acids, was synthesized by solid-phase methodology and correctly folded with three cysteine bridge pairs. The affinities of HEV32 for small chitin fragments—in the forms of N,N′,N′′-triacetylchitotriose ((GlcNAc)$_3$) (millimolar) and N,N′,N′′,N′′′,N′′′′,N′′′′′-hexaacetylchitohexaose ((GlcNAc)$_6$) (micromolar)—as measured by NMR and fluorescence methods, are comparable with those of native hevein. The HEV32 ligand-binding process is enthalpy driven, while entropy opposes binding. The NMR structure of ligand-bound HEV32 in aqueous solution was determined to be highly similar to the NMR structure of ligand-bound hevein.

Solvated molecular-dynamics simulations were performed in order to monitor the changes in side-chain conformation of the binding site of HEV32 and hevein upon interaction with ligands. The calculations suggest that the Trp21 side-chain orientation of HEV32 in the free form differs from that in the bound state; this agrees with fluorescence and thermodynamic data. HEV32 provides a simple molecular model for studying protein–carbohydrate interactions and for understanding the physiological relevance of small native hevein domains lacking C-terminal residues.

Introduction

Interactions between carbohydrates and proteins mediate a broad range of biological activities beginning with fertilization, passing through embryogenesis and tissue maturation, and extending to pathological processes such as tumor metastasis.[1, 2] Many plants respond to pathogenic attack by producing defense proteins,[3, 4] some of these being lectins, carbohydrate-binding proteins that bind reversibly to chitin, a key structural component of the cell walls of fungi and exoskeletons of invertebrates. Chitin is a polysaccharide composed of β(1→4)-linked N-acetylglucosamine (GlcNAc) units (Scheme 1). Most of this kind of lectins include a common structural motif, rich in conserved glycine and cysteine residues and organized around a three-to-five conserved disulfide bond core, usually known as a hevein domain[5] or chitin-binding motif.[6] This domain is present in several plant lectins,[7] such as hevein itself, its natural variant pseudohevein, Urtica dioica agglutinin (UDA), wheat germ agglutinin (WGA), Amaranthus caudatus antimicrobial peptides (Ac-AMP), and also as a component of enzymes with antifungal activity, such as class I chitinases.[8] Surprisingly, some small hevein-containing proteins have remarkable antifungal properties[9] even though they do not have any known enzymatic activity. In humans, hevein is the major allergen of latex and, together with homologous domains, is directly involved in the latex–fruit allergy syndrome.[10, 11]

Elucidation of the mechanisms that govern how oligosaccharides are accommodated in the binding sites of lectins, antibodies, and enzymes is a topic of major interest.[12, 13] From a chemical viewpoint, the amphipathic character of carbohydrates causes different kinds of forces to be involved in their recognition by a given protein.[14–17] Also, there must be a minimum size for a receptor that is able to provide the required 3D structure to support enough specific interactions for ligand recognition.[18] X-ray analyses, NMR spectroscopy, molecular modeling, and calorimetric studies are among the methods that have been widely used to provide detailed structural and

[a] Dr. N. Aboitiz,+ Dr. P. Groves, Dr. J. L. Asensio, Dr. F. J. Cañada,
Prof. Dr. J. Jiménez-Barbero
Department of Protein Structure and Function
Centro de Investigaciones Biológicas, CSIC
Ramiro de Maeztu 9, 28040 Madrid (Spain)
Fax: (+34)91-5531706
E-mail: jcanada@cib.csic.es
        jjbarbero@cib.csic.es

[b] M. Vila-Perelló,+ Prof. Dr. D. Andreu
Department of Experimental and Health Sciences
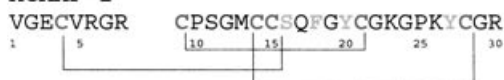Universitat Pompeu Fabra, Doctor Aiguader 80
08003 Barcelona (Spain)

[+] These authors contributed equally to this work.

Supporting information for this article is available on the WWW under http://www.chembiochem.org or from the author: list of the complete set of distance constraints used in the final NMR-based simulated annealing protocol.

HEVEIN

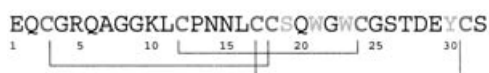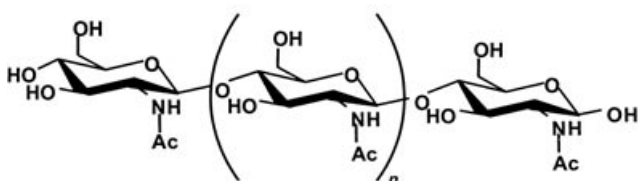EQCGRQAGGKLCPNNLCCSQWGWCGSTDEYCSPDHNCQSNCKD

1   5   10   15   20   25   30   35   40   43

ACAMP-2

VGECVRGR   CPSGMCCSQFGYCGKGPKYCGR

1   5   10   15   20   25   30

HEVEIN-32

EQCGRQAGGKLCPNNLCCSQWGWCGSTDEYCS

1   5   10   15   20   25   30

CHITIN OLIGOMERS

Scheme 1. *Primary sequences of hevein, AcAMP-2, and HEV32, indicating the disulfide bridge pattern. Chemical structures of chitooligosaccharides.*

thermodynamic information on protein–oligosaccharide interactions.[17,19–25]

It seems relevant to verify the relative roles of protein size, structure, and dynamics, as well as the types of interactions involved in the recognition of carbohydrates by proteins. Hevein domains are useful models with which to obtain such information. Hevein-related polypeptides are small and readily available by purification,[26] molecular biology,[27] or peptide synthesis methods.[28,29] X-ray crystallography,[30,31] NMR spectroscopy,[32–35] and calorimetric studies[36] have provided structures for free and bound hevein and thermodynamic data for the complexes. The aromatic residues at relative positions 21, 23, and 30 in hevein stabilize the complexes by means of CH-π stacking interactions[33–35,37] and van der Waals contacts. The hydroxy groups of conserved Ser and Tyr residues (19 and 30 in hevein) are involved in hydrogen-bonding interactions with the carbonyl group of the acetamide moiety and the OH-3 of a GlcNAc residue, respectively.[33–35] The same set of interactions is common to complexes of WGA,[38–40] pseudohevein,[41] Ac-AMP2,[42] the UDA dimer,[43,44] and pokeweed lectin.[45]

In this work we have truncated the C terminus of hevein to obtain a 32-residue peptide (which we call HEV32) by solid-phase synthesis with three disulfide bonds in a similar pattern to Ac-AMP2, but with an approximately 50% sequence homology to this small peptide (Scheme 1). Secondly, the thermodynamic parameters of HEV32 binding to N,N',N''-triacetylchitotriose, (GlcNAc)$_3$, and $N,N',N'',N''',N'''',N'''''$-hexaacetylchitohexaose, (GlcNAc)$_6$, have been determined by NMR and fluorescence measurements. Finally, we have studied the 3D structure of HEV32 complexed with (GlcNAc)$_3$ by NMR spectroscopy and molecular dynamics. A comparison with the corresponding properties of native hevein from latex either in the free or carbohydrate bound form has also been carried out.

The importance of hevein as a major latex allergen and the antifungal activity of Ac-AMP antimicrobial peptides provides additional interest for the study of truncated hevein domains.

Results

Synthesis and folding of HEV32

Our experimental studies rely on an efficient synthesis of the 32-residue, N-terminal sequence of hevein (HEV32). From previous experience, we chose a Boc-based solid-phase synthesis strategy,[46] with formation of the three internal disulfides by oxidation of a hexathiol precursor resulting from acidolysis of 4-methylbenzyl-protected Cys residues. HF treatment of the peptide-resin and reverse-phase HPLC purification led (10% yield) to the fully reduced HEV32 precursor in a highly pure (>95% by HPLC) form, $m/z = 3483.98$ ([M+H]$^+$; calculated 3483.90 Da). Different redox pairs, temperatures, denaturants, pH, and buffers were tested[47,48] in a search for optimal conditions, leading to HEV32 with the native disulfide bond pattern as the major product among 15 possible crosslinked isomers. The optimal protocol consisted of anaerobic oxidation (Ar atmosphere) of the peptide at high dilution (14 μM) in 0.1 M Tris-
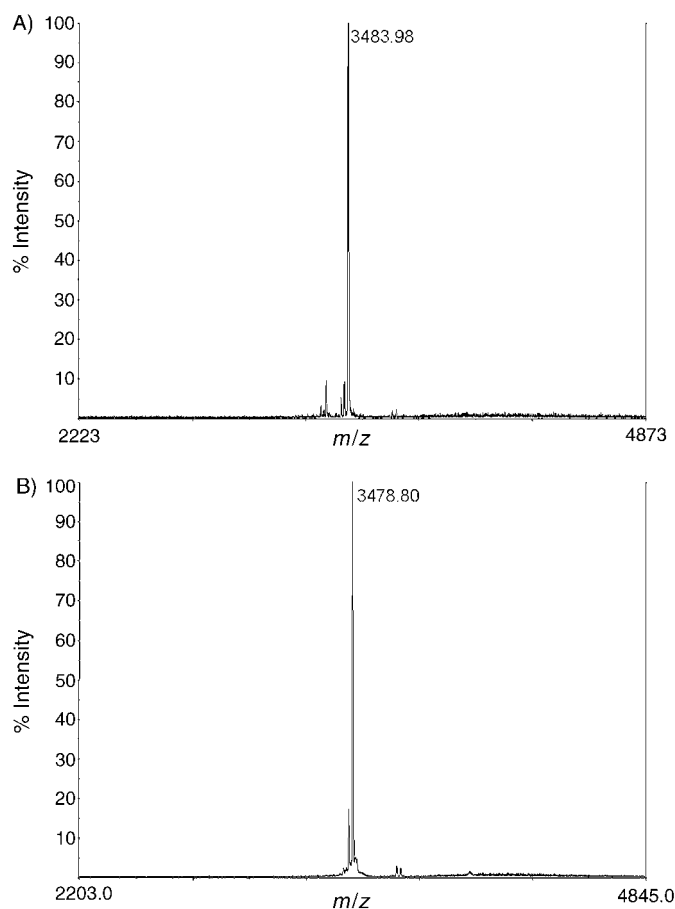
Figure 1. *MALDI-TOF mass spectra of HEV32. A) Reduced HEV32. B) oxidized HEV32, with a molecular mass 6.0 Da lower than the reduced peptide, due to the presence of the three disulfide bonds.*

HCl buffer at pH 8 in the presence of 1 mM EDTA and the redox pair GSH/GSSG to promote thiol/disulfide reshuffling. The reaction was remarkably clean, and after 48 h it was possible to isolate the folded HEV32 in a combined yield (folding and purification) of 34%. The folded peptide had the expected amino acid composition and a molecular mass ($m/z =$ 3478.0, $[M+H]^+$) 6.0 Da lower than that of the fully reduced precursor peptide (Figure 1).

Thermodynamic analysis of HEV32 and hevein binding to chitooligosaccharide ligands

The equilibrium association constants (K_a) were first obtained by 1D ^{1}H NMR titrations. The binding of (GlcNAc)$_3$ to HEV32 and hevein[33–35] was monitored by recording ^{1}H NMR spectra of a series of protein samples in the presence of increasing ligand concentrations. The amide proton signals of Ser19, Trp21, and Trp23 of HEV32 and hevein are all significantly affected by the addition of ligand (Figure 2). The observed effects on chemical shift and line broadening indicate that the interaction is fast on the chemical shift NMR timescale. Variations of more than 0.2 ppm for the chemical shifts of the Ser19 NH proton were monitored and used to determine K_a values for HEV32 (Table 1).

A van't Hoff plot of NMR-determined K_a values as a function of temperature was used to obtain the equilibrium thermodynamic parameters ΔH° and ΔS° (Figure 3, Table 1). It should be noted that although the linear assumption in the van't Hoff plot is only approximate, our previous studies with hevein have demonstrated that the NMR values differ by < 10% from those obtained by isothermal titration microcalorimetry.[33–35]

The entropy of binding, ΔS^0, was found to be negative, as has also been observed for a variety of chitooligosaccharides interacting with hevein itself, pseudohevein, WGA, and UDA.[35, 36, 40, 41, 49] In the current case, the enthalpy values for the binding of (GlcNAc)$_3$ to HEV32 amounted to −62.6 kJ mol^{-1}. Thus, the enthalpy of binding of HEV32 for the trisaccharide is higher than for hevein itself. On the other hand, the entropy loss of HEV32 upon complexation is increased with respect to the natural peptide and reaches a value of −136 J mol^{-1} K^{-1} (Table 1).

Fluorescence spectroscopy was used to obtain independent measurement of K_a values for HEV32 and hevein with (GlcNAc)$_3$ and (GlcNAc)$_6$ (Figure 4). Trp21, Trp23, and Tyr30, all found in
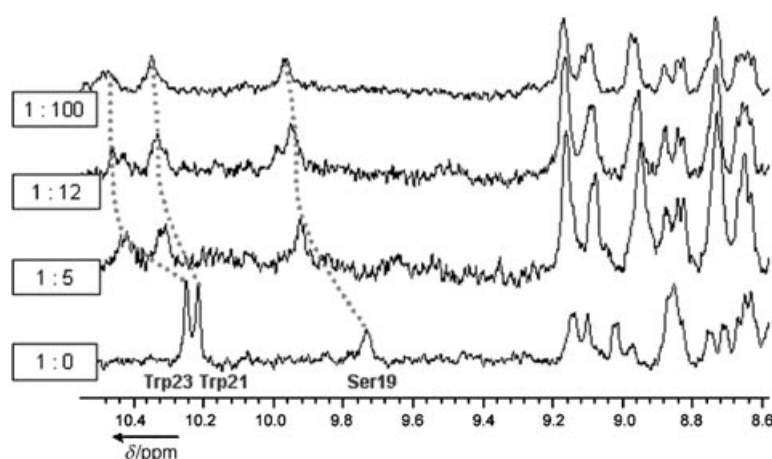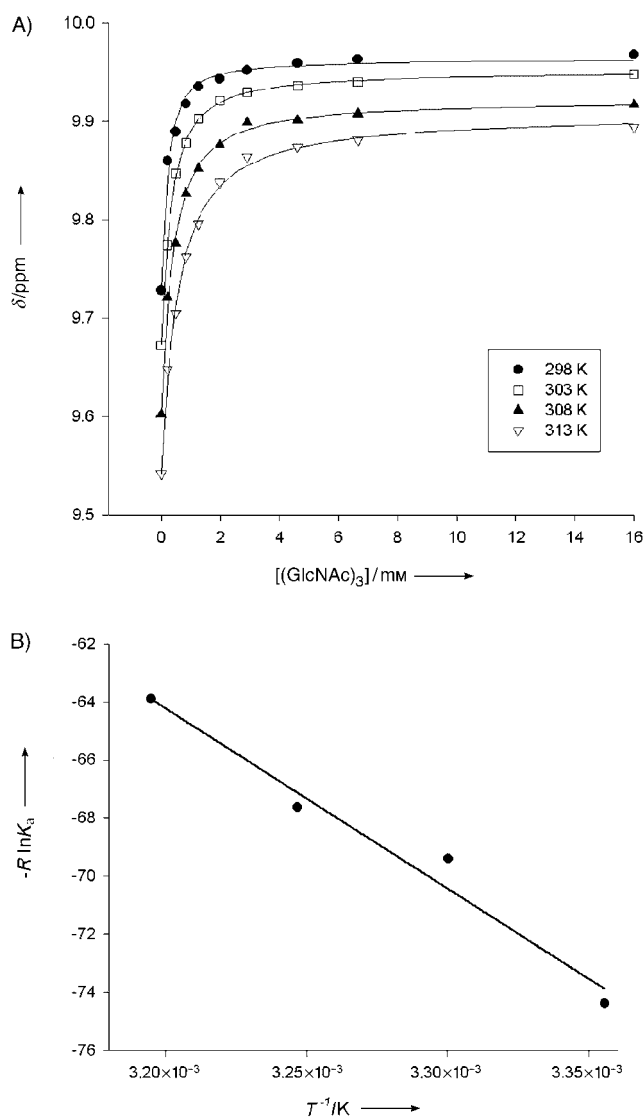

Figure 2. NMR Titration experiment for (GlcNAc)$_3$ binding to HEV32 at 298 K. Low-field protein resonances are shown in the absence (1:0) and in the presence of increased amounts of (GlcNAc)$_3$ (1:5, 1:12, 1:100 ratios). Well-resolved HN resonances that undergo ligand-induced changes in chemical shift are shown by dotted lines.
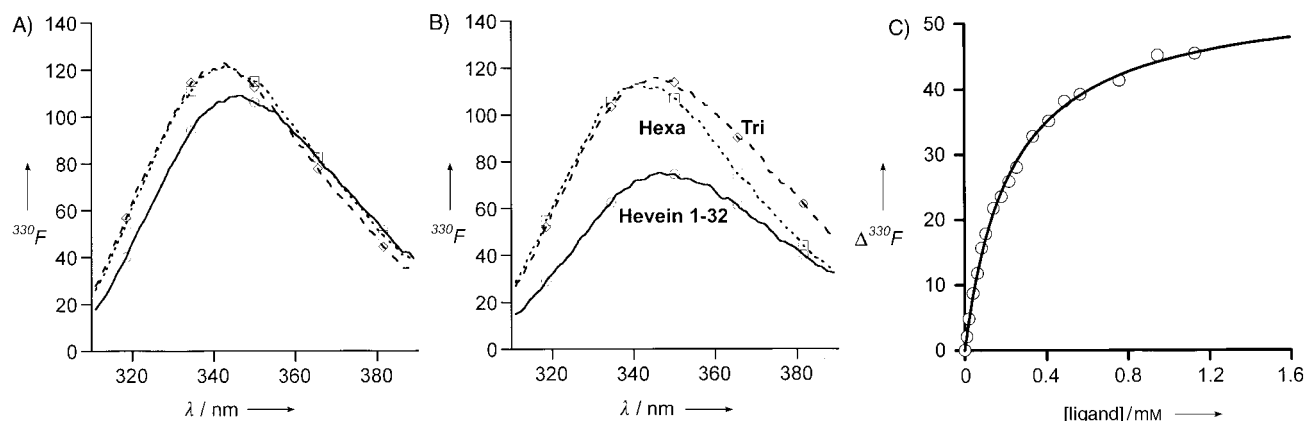
Table 1. Ligand-binding parameters (association constants at different temperatures and corresponding thermodynamic parameters) for hevein and HEV32 as determined by NMR and fluorescence measurements. Van't Hoff values from NMR titrations performed at different temperatures are also given. Titration microcalorimetry values previously obtained for the hevein/(GlcNAc)$_5$ system are also given.

	(GlcNAc)$_3$				(GlcNAc)$_5$
Hevein (NMR)	$\Delta G^\circ = -23.1 \pm 0.4$ kJ mol^{-1}				$\Delta G^\circ = -32.6 \pm 0.5$ kJ mol^{-1}
	$\Delta H^\circ = -36.4$ kJ mol^{-1}				$\Delta H^\circ = -40.1$ kJ mol^{-1}
	$\Delta S^\circ = -44.5$ J K^{-1} mol^{-1}				$\Delta S^\circ = -26.3$ J K^{-1} mol^{-1}
HEV32 (NMR)	$\Delta G^\circ = -21.8 \pm 0.4$ kJ mol^{-1}				
	$\Delta H^\circ = -62.6$ kJ mol^{-1}				
	$\Delta S^\circ = -136.0$ J K^{-1} mol^{-1}				
Hevein (NMR)	298 K	303 K	308 K	318 K	
K_a [M^{-1}]	11 500	8700	6900	5700	
HEV32 (NMR)	298 K	303 K	308 K	313 K	
K_a [M^{-1}]	7700	4200	3400	2200	
	(GlcNAc)$_3$				(GlcNAc)$_6$
Hevein (Fluorescence) 298 K	$\Delta G^\circ = -22.9 \pm 0.4$ kJ mol^{-1} $\Delta^{335}F = +28\%$				$\Delta G^\circ = -33.0 \pm 0.5$ kJ mol^{-1} $\Delta^{335}F = +23\%$
HEV32 (Fluorescence) 298 K	$\Delta G^\circ = -20.7 \pm 0.3$ kJ mol^{-1} $\Delta^{335}F = +89\%$				$\Delta G^\circ = -29.4 \pm 0.4$ kJ mol^{-1} $\Delta^{335}F = +86\%$

the ligand-binding site of hevein domains,[33–35] are the only residues with significant fluorescence properties. The fluorescence titration data were fitted to determine the binding affinities of HEV32 and hevein for (GlcNAc)$_3$ and (GlcNAc)$_6$. An example of a fitted binding curve for HEV32 with (GlcNAc)$_3$ is given in Figure 4C. The ΔG° values are provided in Table 1 for comparison with the NMR data. The fluorescence intensity in the presence of ligand increased by 88% for HEV32 and by 26% for hevein at 335 nm as determined from calculated B_{max} values (Figure 4A and B). Analysis of plots of λ_{max} versus ligand occupancy (not shown) provides a free λ_{max} of 345.6 nm and a bound λ_{max} of 341.2 nm for hevein. Free HEV32 has a λ_{max} of 347.0 nm, which is blue-shifted by 6.5 nm when fully bound by (GlcNAc)$_6$, but is not appreciably shifted in the presence of (GlcNAc)$_3$. The similar λ_{max} data and patterns of ligand-induced

Figure 3. Thermodynamic parameters of (GlcNAc)$_3$-binding to HEV32 determined by NMR. A) Binding curves derived from NMR titrations for the association of (GlcNAc)$_3$ to HEV32. B) van't Hoff plot of lnK$_a$ versus 1/T for HEV32-(GlcNAc)$_3$ complex.

chemical shifts suggest that the ligand-binding modes of HEV32 and hevein are similar.

Three-dimensional structure of HEV32 bound to (GlcNAc)$_3$ based on NMR data

The ^{1}H NMR spectrum of the HEV32:(GlcNAc)$_3$ complex was assigned in aqueous solution. We followed the NOESY/TOCSY protocol (Figure 5) previously used for complexes of hevein, pseudohevein, and the B-domain of WGA.[33–35] The assignment has been deposited in BioMagResBank (entry code 6123).

According to the K_a (Table 1), HEV32 is more than 90% bound with (GlcNAc)$_3$ at 303 K under these experimental conditions. A set of 509 intramolecular protein–protein NOEs were unambiguously assigned and converted into 321 relevant distance constraints (55 intraresidue, 99 sequential, 73 medium, and 94 long-range). Unfortunately, not all the ligand–protein and ligand–ligand NOEs could be unambiguously assigned (Figure 5). Initially only the structure of the peptide in the complex was addressed, and ligand-derived NOEs were not introduced into the structure calculation.

By starting with 500 randomized conformations and applying the DYANA program,[50] a group of 50 structures with low target function values was obtained (Table 2). The 25 best structures from DYANA were subjected to further refinement through a simulated annealing protocol by using the AMBER force field implemented in the AMBER 5.0 package.[51, 52] At this stage, the ligand structure was modeled and introduced into the calculation in a manner based on our previous studies[33–35] and supported by the fluorescence and binding data. Nine intermolecular and four ligand–ligand distances derived from the NOESY spectra were introduced as loose constraints to position the ligand on the protein binding site. The conformation of the ligand was chosen from that deduced for its complex with native hevein[33–35] and hevamine.[53] The structures have been deposited in the Protein Data Bank (entry code 1T0W). The average backbone root mean square deviation (rmsd) of the refined structures was 0.79 Å, while the heavy atom rmsd

Figure 4. Spectra of hevein and HEV32 in the presence and in the absence of chitooligosaccharides (with 80% occupancy). A) Fluorescence spectra of hevein in free (solid line), (GlcNAc)$_3$-bound (dashed line), and (GlcNAc)$_6$-bound (dotted line) states. B) Fluorescence spectra of HEV32 in free (solid line), (GlcNAc)$_3$-bound (dashed line), and (GlcNAc)$_3$-bound (dotted line) states. C) Titration of (GlcNAc)$_3$ into a HEV32 solution followed by tryptophan fluorescence emission (experimental data denoted by circles). The solid line represents the least-squares fit of the data (results provided in Table 1).
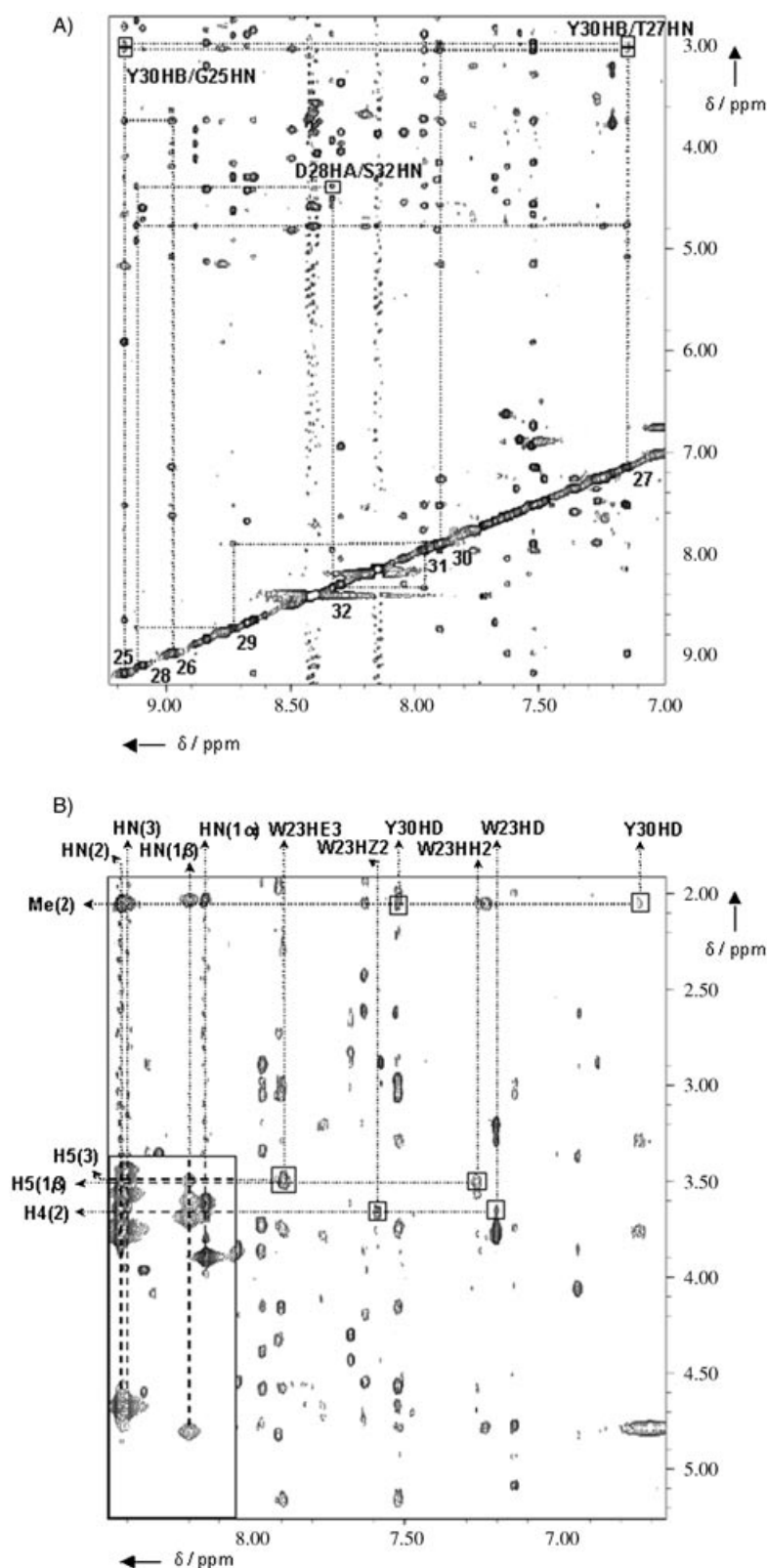
Figure 5. Portions of the 800 MHz NOESY (200 ms mixing time) spectrum of the HEV32/(GlcNAc)$_3$ complex for a 1:6 molar ratio at 298 K. A) Selected protein–protein peaks are highlighted with dotted lines. B) (GlcNAc)$_3$–protein NOEs (dotted lines) are indicated. The inset in the bottom left corner of panel B corresponds to the TOCSY spectrum, in which the saccharide spin systems (dashed lines) can be detected.

was 1.60 Å (residues 3–31, Table 2). The ensemble of 25 structures (Figure 6) exhibited very small deviations from ideal geometry and no non-bonded contacts. Moreover, the only disulfide pattern that allows a 3D structure free from violations is the one corresponding to native hevein, thus confirming the appropriate folding of the synthetic polypeptide.

The two-strand antiparallel β-sheet (between residues 17–18 and 24–25) and α-helical region (29–32), previously described for hevein domains,[18,33–35,42,44] are also observed in the HEV32 complex structure (Figure 7).

## MD-based three-dimensional structure of HEV32 bound to (GlcNAc)$_6$

While the structure of HEV32 was well defined by the NMR data, the few intermolecular NOE and ligand restraints (Figure 5 B) were insufficient to provide a well defined structure for the ligand in the complex. Therefore, a series of solvated molecular dynamics simulations starting from the experimentally derived (NMR) structures was performed in order to obtain, semi-independently,[54–56] a complete view of the 3D structure of the peptide–chitooligosaccharide complex.

Two MD-derived 3D structures of the protein were obtained in the presence (HEV32B) or absence (HEV32F) of a chitooligosaccharide ligand as a way to reveal possible differences between free (HEV32F) and bound (HEV32B) states. In addition, since refined NMR data are available for free and chitooligosaccharide-complexed natural hevein, the same molecular dynamics protocol was also applied to the full-length protein (HEVB and HEVF), firstly to validate the MD approach and secondly to compare both truncated and full-length proteins.

Previous studies proposed an extended binding site in hevein domains, able to accommodate up to six units of GlcNAc, allowing two complementary binding modes for (GlcNAc)$_3$.[35,40] To avoid structural heterogeneity, (GlcNAc)$_6$ was used as a ligand, as it incorporates both binding modes (Figure 8). The solution conformation of (GlcNAc)$_3$ in the free state[53] was taken as a starting point to build the structure of (GlcNAc)$_6$. The conformers are in agreement with the occurrence of the *exo*-anomeric effect and correspond to dihedral angles of $\Phi = 50° \pm 20°$ and $\Psi = 0° \pm 20°$ for the glycosidic linkages. These angles also agree with data obtained from standard NMR methods, molecular mechanics, and dynamics calculations for chitooligosaccharides bound to hevein[33–35] and hevamine.[53] A view of the major conformation of (GlcNAc)$_6$ in solution is also shown in Figure 8. Four MD simulations (Figure 9) were carried out with the AMBER 5.0 package with explicit water molecules, counter-ions, periodic boundary conditions, and
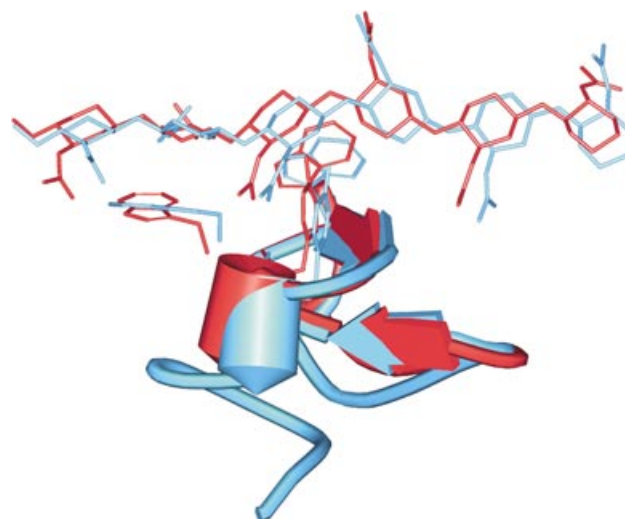
Table 2. Statistics from DYANA and AMBER restrained MD calculations. Limits of variation interval in brackets.

Method	Number of structures	Range	Backbone rmsd [Å]	Heavy atoms rmsd [Å]	Dyana target function	Constraints violated > 0.2 Å (n° structures)	Average sum violation/ structure	Maximum violation/ structure
DYANA	50	3–31	0.68 ± 0.15 (0.22–1.18)	1.20 ± 0.19 (0.68–1.83)	0.34 ± 0.05 (0.20–0.40)	3 (1, 1, 9)	2.2 (1.8–2.6)	0.14–0.22
AMBER	25	3–31	0.79 ± 0.16 (0.00–1.16)	1.60 ± 0.31 (0.00–2.26)				
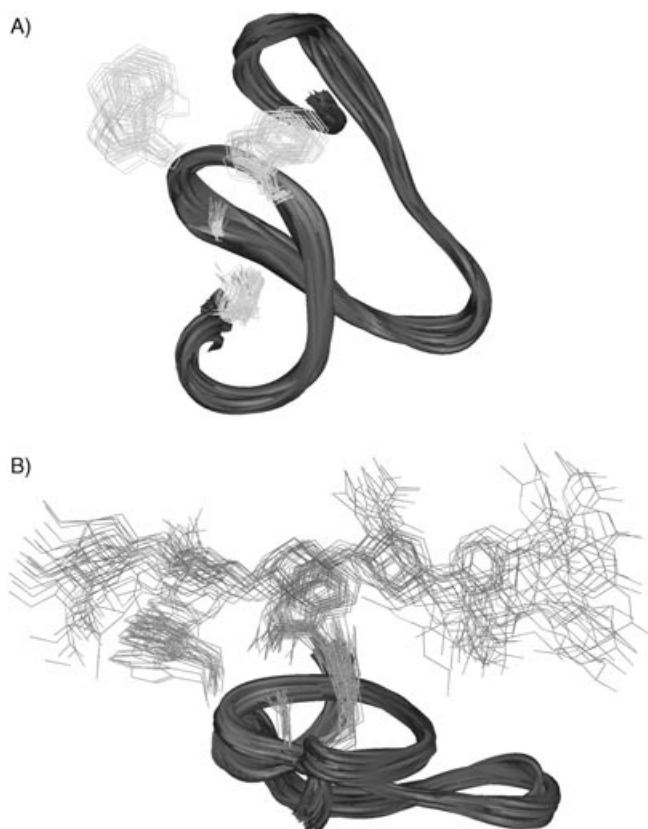
Figure 6. Superimposition of 25 structures calculated from restrained AMBER molecular dynamics simulations with the NOE data obtained for (GlcNAc)$_3$-bound HEV32. A) A view of the protein. The orientations of the key amino acid residues for binding are shown. B) An orthogonal view of the protein with ligand (GlcNAc)$_6$.


Figure 7. Schematic backbone superimposition (residues 3–31) with secondary structure elements of NMR structures of bound HEV32 (red) and bound hevein (blue). Modeled structures of (GlcNAc)$_6$ are shown.

HEVFNMR,[32] and HEVBNMR,[34,35] Table 3) gives a fairly good correlation between the simulated and the experimentally determined data.

After analysis of the four MD simulations (HEVF, HEVB, HEV32F, and HEV32B, Figure 9, Table 3), it was possible to observe that the rmsd for the backbone atoms between residues 3–31 is smaller for hevein than for HEV32 in both the free and the bound states (see Table 3). It seems that truncation of the C terminus modifies the dynamic features of the protein, pro-

Ewald sums for the treatment of electrostatic interactions.[56] No NMR constraints were applied to retain the starting structure of the proteins or to maintain (GlcNAc)$_6$ in contact with the protein. Significantly, (GlcNAc)$_6$ remained within the binding site during the complete duration of the dynamic simulations of the complexes. Comparison with the experimentally derived NMR structures (HEV32BNMR,

Table 3. Rmsd values (Å) for the 4.5 ns MD simulations of free hevein (HEVF), bound hevein (HEVB), free HEV32 (HEV32F), and bound HEV32 (HEV32B). Comparison with the experimentally derived (NMR) structures for bound HEV32 (NMRHEV32B) and free (NMRHEVF)[32] and bound hevein (NMRHEVB).[35] Superimposition range is 3–31 in all cases.

System	Backbone rmsd (3–31) [Å]	rmsd for key lateral chains Ser19/Trp21/Trp23/Tyr30	Pairwise rmsd (3–31) [Å] Systems	rmsd
HEVF	0.45 ± 0.11	0.38/0.32/0.33/0.37	HEVF/HEVB	0.73
			HEVF/HEV32F	1.43
			HEVF/NMRHEVF	1.06
HEVB	0.39 ± 0.10	0.19/0.28/0.32/0.30	HEVB/NMRHEVB	0.58
NMRHEVB	0.63 ± 0.17	0.16/0.34/0.20/0.30	NMRHEVB/NMRHEV32B	0.94
HEV32F	0.73 ± 0.16	0.49/0.47/0.40/0.41	HEV32F/HEV32B	1.44
HEV32B	0.58 ± 0.12	0.19/0.41/0.31/0.36	HEV32B/HEVB	0.71
NMRHEV32B	0.65 ± 0.18	0.32/0.45/0.21/0.38	NMRHEV32B/NMRHEVF	1.11
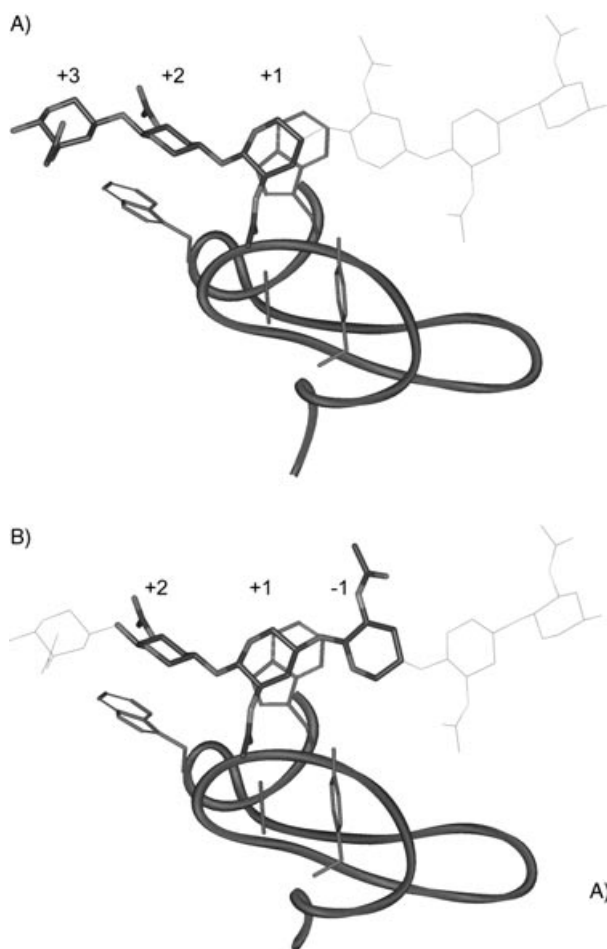
Figure 8. *MD simulation of HEV32 bound to (GlcNAc)$_6$. The protein binding site can host GlcNAc units on the labeled positions −1, +1, +2, and +3. For a given (GlcNAc)$_3$, highlighted in stick representation in the figure, either the central unit (panel A) or the reducing end (panel B) may interact with Trp21. The conformation around all glycosidic linkages (syn-Φψ) complies with the exoanomeric orientation and is in agreement with the published NMR data for chitooligosaccharides.*

ducing a more flexible peptide. Interestingly, complex formation only marginally modifies the backbone rmsd for hevein, by 13 %. In contrast, complexation gives rise to a much better definition of the backbone of HEV32, with a 25 % decrease in the rmsd.

Discussion

Refolding of synthesized HEV32

The native hevein disulfide pattern of HEV32 was supported by the ligand affinities (Table 1) and confirmed by the NMR structure determination (Figure 6). The efficient preparation of a synthetic truncated hevein supports the hypothesis that the N-terminal domain can form a structurally and functionally autonomous entity. The folding of HEV32 is anal-

ogous to the results obtained by Muraki et al.[28, 29] with a full length, synthetic chitin-binding domain.

Thermodynamic analysis of HEV32 and hevein binding to chitooligosaccharide ligands

The $\Delta G°$ values for hevein binding to (GlcNAc)$_3$, based on fluorescence and NMR data (Table 1), are very similar to ΔG measured by isothermal titration calorimetry (−22.2 kJ mol^{-1}).[33–35] The ΔG of HEV32 for (GlcNAc)$_3$ is 1.3 (NMR) and 2.2 kJ mol^{-1} (fluorescence) weaker than the corresponding value for hevein (Table 1). The ligand-induced blue shift in λ_{max} values and the increase in fluorescence intensity of HEV32 and hevein are similar to those reported for WGA.[39, 57] These data confirm the consistency of our results with literature data and indicate a typical hevein binding mode for HEV32. Comparison of (GlcNAc)$_6$ binding data shows that truncation of hevein leads to a loss of 3.6 ± 0.7 kJ mol^{-1} in $\Delta G°$. These data suggest that the C terminus of hevein does not appear to make a significant contribution to the overall binding affinity of chitooligosaccharide ligands. Although the measured K_a values are in the same range as those of natural hevein, the van't Hoff data show a larger $\Delta H°$ value for HEV32 compensated for by an increased $\Delta S°$ that strongly opposes association, as shown in Table 1. Although the origin of this enthalpy–entropy compen-
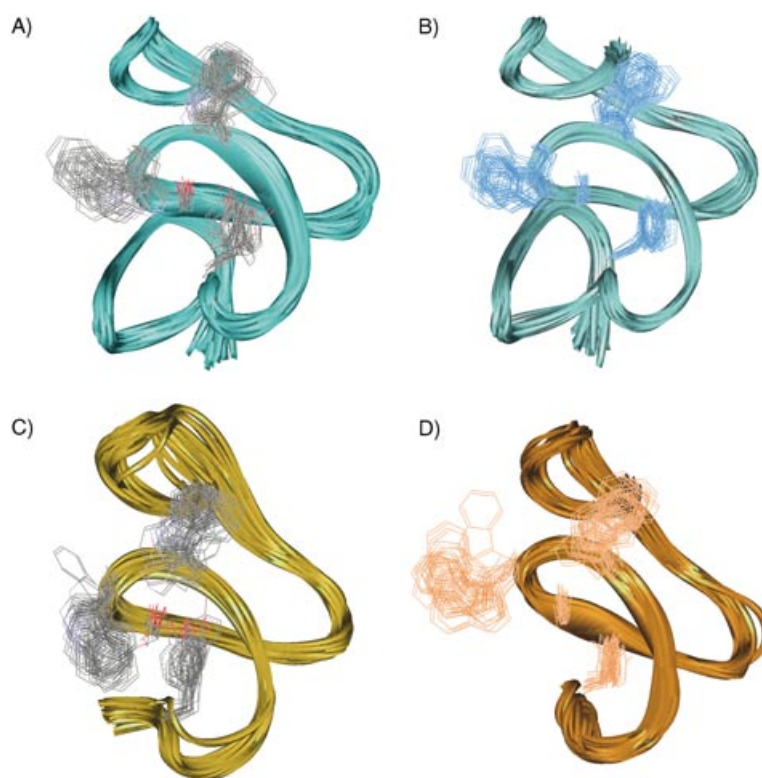
Figure 9. *Backbone superimposition (residues 3–31) of 24 structures (taken each ≈ 200 ps) from the 4.5 ns solvated AMBER MD simulations for free and bound hevein. A) Free hevein (HEVF, rmsd 0.448 Å). B) Chitohexaose-bound hevein (HEVB, rmsd 0.395 Å). C) Free HEV32 (HEV32F, rmsd 0.731 Å). D) Chitohexaose-bound HEV32 (HEV32B, rmsd 0.581 Å). The interaction of the C terminus of hevein with the Trp21 region may be observed in panels A and B. This interaction is absent in the truncated mutant (panels C and D).*

sation phenomenon remains an open question,[58–60] it has been reported,[61] for this magnitude and sign of ΔS and ΔH, that hydrogen bonding and van der Waals forces should be the most important factors that stabilize the complex. Part of the observed negative entropy of binding could arise from rigidification of the carbohydrate and/or protein lateral chains,[59,60] or by reorganization of the water structure.[58] As deduced in earlier studies,[33–35] the maximum loss of conformational entropy by freezing of the (GlcNAc)$_3$ ligand upon binding to lectin domains can reach 17 kJ mol^{-1} at 25 °C (conformational entropy estimated from the conformational distribution map of (GlcNAc)$_3$[33–35])—less than the value of 40.8 kJ mol^{-1} at 25 °C determined for HEV32. Therefore, it seems that the smaller truncated domain must pay an entropic penalty with some reduction of the lateral chains' flexibility upon binding in order to better accommodate the trisaccharide, and providing a more favorable binding enthalpy.
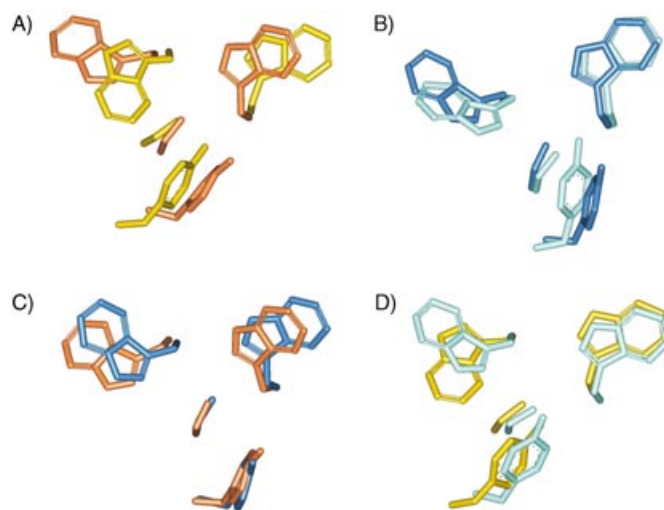
Comparison of HEV32 and hevein structures

Fluorescence resonance energy transfer (FRET)[62] would be expected to provide a large contribution to the fluorescence intensity, as Tyr30 (a FRET donor) is held 10–15 Å from Trp21 and Trp23 (FRET acceptors). The similar fluorescence spectra of ligand-bound HEV32 and hevein suggest that aromatic residues enjoy similar degrees of solvent exposure, relative inter-residue distances and orientations. This is not the case for free HEV32 and free hevein, the fluorescence spectra of which are distinct. The slightly longer wavelength λ_{max} (by 1.4 nm) and greater degree of solvent quenching in HEV32 in relation to hevein is consistent with: i) loss of packing between the tyrosine and tryptophan residues leading to a larger solvent exposed area, ii) longer mean distances between the tyrosine donor and one or both tryptophan residues, and iii) different relative orientations of the FRET donor and acceptors. It is not possible to factorize these contributions from the fluorescence data alone. However, each factor is revealed in the NMR and MD models of the free and bound proteins.

The NMR-derived 3D structure of HEV32 within the complex (NMRHEV32B, Figure 7) in aqueous solution at pH 5.6 is very similar (rmsd 0.94 Å, residues 3–31, and 0.63 Å for residues 16–30) to that previously deduced by NMR methods for hevein complexed with chitooligosaccharide ligand in aqueous solution (NMRHEVB, Figure 7),[33–35] to hevein in the free state, PDB ID: 1HEV, (NMRHEVF, rmsd, 1.11 Å) and to the X-ray structure of hevein recently deposited in the Protein Data Bank (PDB ID: 1Q9B, rmsd, 0.833 Å).

From the rmsds of the backbone computed from the solvated MD simulations, the structure of hevein is very similar in the free and the bound states. The MD rmsds are lower than the corresponding NMR rmsds, and this indicates the importance of including water molecules in the simulation analysis. The NMR and MD structures of the complexes for hevein (HEVB) and HEV32 (HEV32B) are remarkably similar. Both proteins adopt well defined structures within their complexes that are better organized (lower rmsds) than the free protein structures.

Larger differences in the protein structures are observed when the side chain conformations are taken into account. The hydrophobic patch formed by the three aromatic residues is of primary interest (Figure 10). It adopts a precise geometry in both protein complexes that allows the patches to be cov-

Figure 10. Comparison of free and ligand-bound MD structures for HEV32 and hevein, as deduced from the corresponding 4.5 ns MD simulations. The structures are backbone-superimposed (residues 3–31). Side chains of the amino acids involved in ligand-binding—Ser19, Trp21, Trp23, and Tyr30—are shown in stick representation. A) HEV32F (yellow) and HEV32B (brown), maximum variation of side chain position occurs for Trp21. B) HEVF (light blue) and HEVB (blue). C) HEVB (blue) and HEV32B (brown). D) HEVF (light blue) and HEV32F (yellow).

ered by the chitooligosaccharide chain (Figure 10 A). The geometry of the hydrophobic patch is largely retained in the free hevein MD structures (HEVF), reflecting the fact that the binding site has been found to be preorganized in hevein domains.[33–35] However, Trp21 adopts a wider range of side-chain conformations in the free HEV32 MD structures (HEV32F) (Figure 10 B). This is reflected in the comparison of rmsd values for HEV32 and hevein in their free and bound forms (either NMR or MD structures) (Table 3, Figure 10).

The rmsds of the three key aromatic amino acid residues of HEV32 implicated in binding (Trp21, Trp23, and Tyr30) show differences between the free and the bound states, with Trp21 having the largest difference in rmsd (0.09 versus 0.05 or 0.06 Å, Table 3). Smaller differences are observed for full-length hevein. Trp21 is adjacent to the C terminus of hevein. To conclude, the loss of the C terminus from hevein appears to be the source of the conformational mobility of Trp21 in HEV32 and the resulting differences in thermodynamic and fluorescence properties for HEV32 in relation to hevein.

According to the NMR and MD data, both van der Waals and polar interactions contribute to hevein and HEV32 complex formation, stabilizing the position of the carbohydrate rings through the formation of hydrogen bonds and π-stacking interactions with aromatic side chains. NMR, X-ray crystallography, and thermodynamic measurements have convincingly

documented that these interactions are key features for the establishment of protein–carbohydrate complexes.[6,33–44,63,64]

Conclusion

The interaction of HEV32 with chitooligosaccharides has been described in structural terms, with use being made of a NMR-derived 3D structure and a modeling procedure. We have shown that the binding process is enthalpically driven and that both hydrogen bonds and van der Waals forces contribute to the stability of the complexes in aqueous solution. In contrast to the native protein, the orientations of the amino acid residues of HEV32 implicated in binding are alterered upon complexation. Therefore, the environment of the binding site is significant for prediction of the impact of changes in their constitutions for binding affinity. Our data support the physiological relevance of small native hevein domains (such as the native Ac-AMP2) that lack C-terminal residues analogous to hevein 33–43. In principle, the loss of the C terminus is consistent with a small disorganization of the three aromatic residues that provide the main chitin binding site. The role of the C terminus might be related to other factors, such as selectivity or a function as a spacer between hevein and other domains of chitinases. Further modifications in the electronic and lipophilic nature of the aromatic rings of hevein domains and their impact on carbohydrate binding are currently underway in our laboratory.

Experimental Section

Source of lectin and ligand: Boc-protected amino acids and *p*-methylbenzhydrylamine resin (MBHA) were from Neosystems (Strasbourg, France) and Bachem (Bubendorf, Switzerland), respectively. Dichloromethane (DCM) and dimethylformamide (DMF) for peptide synthesis, and HPLC-grade acetonitrile (MeCN) were from SDS (Peypin, France). Trifluoroacetic acid (TFA), diisopropylethylamine (DIEA), and other chemicals were from Sigma–Aldrich.

Instrumentation: HPLC preparative and analytical separations were performed with Waters Delta PREP 4000 and Shimadzu LC-6A systems, respectively. Amino acid analysis of peptide hydrolysates (6 N HCl, 155°C, 1 h) were run on a Beckman 6300 analyzer. MALDI-TOF mass spectra were acquired on a Voyager DE-STR spectrometer (Applied Biosystems) in the linear mode by using α-cyano-4-hydroxycinnamic acid for the matrix. NMR: 1D and 2D spectra were recorded on 500 MHz Varian UNITY, and Bruker Avance 500 and 800 MHz spectrometers. Fluorescence experiments were performed on a Hitachi F-2500 spectrometer at 298 K (maintained with a Julaba F-12 temperature control unit).

Peptide synthesis: The 32-amino acid sequence of HEV32 was assembled as a C-terminal carboxamide on a MBHA resin by standard Boc solid-phase peptide synthesis protocols, in the manual mode. The original resin substitution (0.70 mmol g^{-1}) was lowered (0.30 mmol g^{-1}) by substoichiometric coupling of Boc-Ser(Bzl)-OH (0.5 equiv), followed by capping with acetic anhydride. The synthetic cycle included Boc deprotection with TFA/DCM (40% *v/v*, 1 + 20 min, 25°C), neutralization with DIEA/DCM (5% *v/v*, 5×1 min) and Boc-amino acid coupling in the presence of 2-(1*H*-benzotriazol-1-yl)-1,1,3,3-tetramethyluronium tetrafluoroborate (TBTU) and DIEA (4, 4, and 8 equivalents, respectively) for 30 min, 25°C, plus

DCM and DMF washes. Amino acid side chains were protected with benzyl (Ser, Thr), 2-bromobenzyloxycarbonyl (Tyr), 2-chlorobenzyloxycarbonyl (Lys), cyclohexyl (Asp, Glu), formyl (Trp), 4-methylbenzyl (Cys), tosyl (Arg), and xanthyl (Asn, Gln) groups. After chain assembly, the *N*-terminal Boc group was removed (40% (*v/v*) TFA)/DCM, 1 + 20 min, 25°C), and the peptide-resin was washed with DCM and DMF, treated with piperidine/DMF (1:1 *v/v*; 1 + 20 min, 25°C) to remove the formyl group, washed, and air-dried. The peptide was then fully deprotected and cleaved from the resin by acidolysis with anhydrous HF/*p*-cresol (9:1 *v/v*, 1 h, 0°C). The crude hexathiol peptide was taken up in 10% AcOH, lyophilized, and purified by reverse-phase HPLC on Kromasil C8 (Akzo Nobel, 2×25 cm, 10 µm, 100 Å pore size), by use of a 15–50% linear gradient of 0.1% (*v/v*) TFA/MeCN into 0.1% TFA/water over 120 min at 25 mL min^{-1}. The purity and identity of the different fractions were assessed by analytical HPLC and by amino acid analysis and MALDI-TOF mass spectrometry, respectively. Fractions judged to be of sufficient purity (> 95% by HPLC) were pooled, lyophilized, and used for oxidative folding.

In the optimal folding protocol, the hexathiol peptide was dissolved at 14 µM (0.1 M Tris-HCl, 1 mM EDTA, pH 8) under an Ar atmosphere in the presence of reduced (GSH) and oxidized glutathione (GSSG) to give a peptide/GSH/GSSG ratio of 1:100:10. After gentle stirring for 48 h at 25°C, and when the Ellman test[65] of the major HPLC product was negative, the reaction mixture was quenched by TFA addition and then directly loaded onto a preparative reverse-phase HPLC system (see above) and purified by use of a linear 5–35% gradient of 0.1% TFA/MeCN into 0.1% TFA/water over 75 min. The peptide was further characterized by MALDI-TOF mass spectrometry and amino acid analysis. Oligosaccharides were purchased from Toronto Research Chemicals, Canada.

NMR titration experiments: The binding of the carbohydrate to hevein and HEV32 was monitored by recording of 1D 500 MHz ^{1}H NMR spectra of a series of samples at increasing ligand concentration (ten different concentrations) as previously described.[33–35] The concentration of the protein during the experiments was kept constant (ca. 0.18 mM). The samples were prepared by dissolving the lyophilized protein in buffer (^{1}H$_2$O/^{2}H$_2$O 85:15, 100 mM NaCl, 20 mM NaH$_2$PO$_4$, pH 5.6, 1.0 mL). The 1D NMR spectrum for the sample with the highest ligand/protein ratio was recorded by dissolving the corresponding oligosaccharide (16 mM) in the lectin-containing solution described above (0.5 mL). The titration curve was established by addition of small aliquots of the highest ligand/protein ratio sample to the ligand-free protein sample as previously described Thermodynamic equilibrium parameters, ΔS and ΔH, for the protein–(GlcNAc)$_3$ interaction were determined from van't Hoff plots in which the affinity constants were assessed at 25, 30, 35, and 40°C.

Two-dimensional NMR experiments: The spectra were recorded at 500 and 800 MHz. The sample HEV32/(GlcNAc)$_3$ complex (1:6 molar ratio, 0.5 mM protein concentration) was prepared in H$_2$O/D$_2$O, 85:15, 100 mM NaCl, 20 mM NaH$_2$PO$_4$, pH 5.6 solution and degassed by passage of argon. TOCSY[66] (80 ms mixing time) was performed by use of standard sequences at 298 K. 2D NOESY experiments[67] were performed with mixing times of 200 and 300 ms at 298 K.

Structure calculations: The torsion angle dynamics protocol, as implemented in the DYANA[68] package, was followed. Upper limits for proton–proton distances were obtained from NOESY cross-peak intensities at two mixing times (200 and 300 ms). Cross-peaks were

classified as strong, medium, and weak, corresponding to upper limits of 2.6, 3.5, and 5.5 Å. The lower limit for proton–proton distances was set as the sum of the van der Waals radii of the protons. Constraints involving diastereoisomeric atoms were defined to an intermediate position (pseudoatom) and assigned an additional distance of 2.20 Å. Disulfide linkages were included as distance constraints between S–S (2.0 Å $< r <$ 2.1 Å) and between Cβ–S (3.0 Å $< r <$ 3.1 Å). Distance geometry calculations were performed on a Linux PC computer by use of DYANA. A set of 321 distance constraints derived from protein–protein NOEs, plus 13 implied distance restraints relating to the ligand, were used in the final round of calculations. The 25 best DYANA structures in terms of target function were subjected to restrained molecular dynamics[69] with the AMBER[52] force field. After an initial restrained energy minimization (REM) with 2000 conjugate gradient iterations, the structures were equilibrated at 600 K for 2 ps and, at this temperature, their conformational behavior for the next 2 ps was simulated by restrained molecular dynamics (RMD). In the next step, the structures were subjected to a cooling regime, in which the temperature was decreased by 100 K every 2 ps until a temperature of 100 K was reached. At this temperature, 4 ps of RMD calculations were carried out. The final structures were energy-minimized (REM) by use of 2000 conjugate gradient iterations. The refined structures can be found in the Protein DataBank (PDB ID: 1T0W).

Molecular mechanics and dynamics calculations: Φ is defined as H-1''-C-1''-O-C4'/H-1'-C-1'-O-C4 and Ψ as C1''-O-C4'-H4' C⁻1'-O-C4-H4 for the non-reducing-middle and middle-reducing disaccharide entities respectively. The MD calculations for the complexes were performed by use of the AMBER 5.0 package.[52] Atomic charges for the chitooligosaccharides in the MD simulations of the complexes were AMBER charges. Starting glycosidic torsion angles were taken from the MM3* calculations for (GlcNAc)₃. The input files were prepared from the NMR-derived structures by use of the X-LEAP module of the AMBER package. The obtained initial structures were immersed in a box of 3017 TIP3P water molecules in order to obtain accurate solvation. Cutoff for nonbonding interactions was set to 11.0 Å. The molecular dynamics simulations were carried out with the Sander module and were performed by use of periodic boundary conditions and the particle-mesh Ewald approach to introduce long-range electrostatic effects. The SHAKE algorithm for hydrogen atoms, which used a 2 fs time step, was employed.

All simulations (HEVF, HEVB, HEV32F, and HEV32B) were performed at constant pressure and temperature, with use of the Berendsen coupling algorithm for the latter. Equilibration of the system was carried out as follows: as a first step, a short minimization with positional restraints on solute atoms was run to remove any potentially bad contacts. The force constant for the positional constraints was 500 Kcal mol⁻¹ Å. Next a 12.5 ps molecular dynamics calculation was run at 300 K with maintaining of positional restraints on the ligand in order to equilibrate the water box and ions. A 9 Å cutoff was used for the treatment of the electrostatic interactions. The system was further equilibrated (12.5 ps run at 300 K) by use of the mesh Ewald approach for long-range electrostatic effects. Then, the system was subjected to several minimization cycles (each using 1000 steepest descent iterations) gradually reducing positional restraints on the chitooligosaccharides from 500 Kcal mol⁻¹ Å to 0. Finally, MD trajectories at constant pressure (1 atm) and temperature (300 K) were collected and analyzed by use of the Carnal module of AMBER. Structures were recorded every 0.5 ps for a total calculation time of 4.5 ns in all cases.

Fluorescence samples: The concentrations of stock hevein and HEV32 were calculated by UV based on calculated $^{280}\varepsilon$ values of 13140 and 13020 M⁻¹ cm⁻¹, respectively.[70] Fluorescence experiments were performed with hevein (9.2×10^{-7} M) and HEV32 (6.0×10^{-7} M), with corrections to account for the different protein concentrations. The stock chitooligosaccharide concentrations were calculated by weight.

Emission fluorescence: Experimental parameters were $\lambda_{ex} =$ 280 nm, λ_{em} scanned between 310 and 390 nm over 120 s, excitation and emission slits of 5 nm and datapoints collected each 0.5 nm. Experiments were performed in buffer (0.1 M NaCl, 0.02 M NaH₂PO₄, pH 5.6, 2 mL). Chitooligosaccharide solution (14–18 aliquots) was added to the protein solutions, and protein dilution, up to 7%, was corrected. Titration data were followed at a fixed wavelength of 335 nm, providing the maximum difference between bound and free protein spectra. Titration data were least-squares fitted in Sigmaplot v8.02 (SPSS Inc., USA) by use of a curve-fitting routine that corrects for bound protein concentration.

[1] H.-J. Gabius, S. Gabius in *Glycosciences: Status and Perspectives*, Chapman & Hall, London, **1997**.
[2] H. Rudiger, H. C. Siebert, D. Solis, J. Jimenez-Barbero, A. Romero, C. W. von der Lieth, T. Diaz-Marino, H. J. Gabius, *Curr. Med. Chem.* **2000**, *7*, 389–416.
[3] W. J. Peumans, E. J. M. van Damme, *Histochem. J.* **1995**, *27*, 253–271.
[4] F. Garcia-Olmedo, A. Molina, J. M. Alamillo, P. Rodriguez-Palenzuela, *Biopolymers* **1998**, *47*, 479–491.
[5] A. Rodriguez, M. Tablero, B. Barragan, P. Lara, M. Rangel, B. Arreguin, L. Posan, M. Soriano-Garcia, *J. Crystal Growth* **1986**, *76*, 710–714.
[6] H. T. Wright, G. Sandrasegaram, C. S. Wright, *J. Mol. Evol.* **1991**, *33*, 283–294.
[7] E. J. M. Van Damme, W. J. Peumans, A. Barre, P. Rouge, *Crit. Rev. Plant Sci.* **1998**, *17*, 575–692.
[8] J. J. Beintema, *FEBS Lett.* **1994**, *350*, 159–163.
[9] J. Vanparijs, W. F. Broekaert, I. J. Goldstein, W. J. Peumans, *Planta* **1991**, *183*, 258–264.
[10] H. Alenius, N. Kalkkinen, T. Reunala, K. Turjanmaa, T. Palosuo, *J. Immunol.* **1996**, *156*, 1618–1625.
[11] C. Blanco, A. Diaz-Perales, C. Collada, R. Sanchez-Monge, C. Aragoncillo, R. Castillo, N. Ortega, M. Alvarez, T. Carrillo, G. Salcedo, *J. Allergy Clin. Immunol.* **1999**, *103*, 507–513.
[12] H. Lis, N. Sharon, *Chem. Rev.* **1998**, *98*, 637–674.
[13] W. J. Peumans, A. Barre, Q. Hao, P. Rouge, E. J. M. van Damme, *Trends Glycosci. Glycotechnol.* **2000**, *12*, 83–101.
[14] F. A. Quiocho, *Pure Appl. Chem.* **1989**, *61*, 1293–1306.
[15] H.-J. Gabius, *Pharm. Res.* **1998**, *15*, 23–30.
[16] D. Solis, J. Jimenez-Barbero, H. Kaltner, A. Romero, H. C. Siebert, C. W. von der Lieth, H. J. Gabius, *Cells Tissues Organs* **2001**, *168*, 5–23.

FULL PAPERS

[17] T. K. Dam, F. Brewer, *Chem. Rev.* **2002**, *102*, 387 – 429.

[18] H. C. Siebert, S. Y. Lu, M. Frank, J. Kramer, R. Wechselberger, J. Joosten, S. Andre, K. Rittenhouse-Olson, R. Roy, C. W. von der Lieth, R. Kaptein, J. F. Vliegenthart, A. J. Heck, H. J. Gabius, *Biochemistry* **2002**, *41*, 9707 – 9717.

[19] C. von der Lieth, H. Siebert, T. Kozar, M. Burchert, M. Frank, M. Gilleron, H. Kaltner, G. Kayser, E. Tajkhorshid, N. V. Bovin, J. F. Vliegenthart, H. J. Gabius, *Acta Anat. (Basel).* **1998**, *161*, 91 – 109.

[20] R. Woods, *Glycoconj. J.* **1998**, *15*, 209 – 216.

[21] J. Jimenez-Barbero, J. L. Asensio, F. J. Canada, A. Poveda, *Curr. Opin. Struct. Biol.* **1999**, *9*, 549 – 555.

[22] A. Imberty, S. Perez, *Chem. Rev.* **2000**, *100*, 4567 – 4588.

[23] C. A. Bewley, *Structure Fold Des.* **2001**, *9*, 931 – 940.

[24] M. R. Wormald, A. J. Petrescu, Y. L. Pao, A. Glithero, T. Elliott, R. A. Dwek, *Chem. Rev.* **2002**, *102*, 371 – 386.

[25] H. Kogelberg, D. Solis, J. Jimenez-Barbero, *Curr. Opin. Struct. Biol.* **2003**, *13*, 646 – 653.

[26] B. L. Archer, *Biochem. J.* **1960**, *75*, 236 – 240.

[27] P. Karisola, J. Mikkola, N. Kalkkinen, K. J. Airenne, O. H. Laitinen, S. Repo, O. T. Pentikainen, T. Reunala, K. Turjanmaa, M. S. Johnson, T. Palosuo, M. S. Kulomaa, H. Alenius, *J. Immunol.* **2004**, *172*, 2621 – 2628.

[28] M. Muraki, H. Morii, K. Harata, *Protein Pept. Lett.* **1998**, *5*, 193 – 198.

[29] M. Muraki, M. Morii, K. Harata, *Protein Eng.* **2000**, *13*, 385 – 389.

[30] A. Rodriguez-Romero, K. G. Ravichandran, M. Soriano-Garcia, *FEBS Lett.* **1991**, *291*, 307 – 339.

[31] C. A. Reyes-Lopez, A. Hernandez-Santoyo, M. Pedraza-Escalona, G. Mendoza, A. Hernandez-Arana, A. Rodriguez-Romero, *Biochem. Biophys. Res. Commun.* **2004**, *314*, 123 – 130.

[32] N. H. Andersen, B. Cao, A. Rodriguez-Romero, B. Arreguin, *Biochemistry* **1993**, *32*, 1407 – 1422.

[33] J. L. Asensio, F. J. Canada, M. Bruix, A. Rodriguez-Romero, J. Jimenez-Barbero, *Eur. J. Biochem.* **1995**, *230*, 621 – 633.

[34] J. L. Asensio, F. J. Canada, M. Bruix, C. Gonzalez, N. Khiar, A. Rodriguez-Romero, J. Jimenez-Barbero, *Glycobiology* **1998**, *8*, 569 – 577.

[35] J. L. Asensio, F. J. Canada, H. C. Siebert, J. Laynez, A. Poveda, P. M. Nieto, U. M. Soedjanaamadja, H. J. Gabius, J. Jimenez-Barbero, *Chem. Biol.* **2000**, *7*, 529 – 543.

[36] E. Garcia-Hernandez, R. A. Zubillaga, A. Rojo-Dominguez, A. Rodriguez-Romero, A. Hernandez-Arana, *Proteins* **1997**, *29*, 467 – 477.

[37] M. Muraki, *Protein Pept. Lett.* **2002**, *9*, 195 – 209.

[38] C. S. Wright, G. E. Kellogg, *Protein Sci.* **1996**, *5*, 1466 – 1476.

[39] G. Bains, R. T. Lee, Y. C. Lee, E. Freire, *Biochemistry* **1992**, *31*, 12624 – 12628.

[40] J. F. Espinosa, J. L. Asensio, J. L. Garcia, J. Laynez, M. Bruix, C. Wright, H. C. Siebert, H. J. Gabius, F. J. Canada, J. Jimenez-Barbero, *Eur. J. Biochem.* **2000**, *267*, 3965 – 3978.

[41] J. L. Asensio, H. C. Siebert, C. W. von der Lieth, J. Laynez, M. Bruix, U. M. Soedjanaamadja, J. J. Beintema, F. J. Canada, H. J. Gabius, J. Jimenez-Barbero, *Proteins* **2000**, *40*, 218 – 236.

[42] J. C. Martins, D. Maes, R. Loris, H. A. Pepermans, L. Wyns, R. Willem, P. Verheyden, *J. Mol. Biol.* **1996**, *258*, 322 – 333.

[43] F. A. Saul, P. Rovira, G. Boulot, E. J. Damme, W. J. Peumans, P. Truffa-Bachi, G. A. Bentley, *Structure Fold Des.* **2000**, *8*, 593 – 603.

[44] K. Harata, M. Muraki, *J. Mol. Biol.* **2000**, *297*, 673 – 681.

[45] M. Hayashida, T. Fujii, M. Hamasu, M. Ishiguro, Y. Hata, *J. Mol. Biol.* **2003**, *334*, 551 – 565.

[46] T. S. Yokum, G. Barany, in *Solid-Phase Synthesis* (Eds.: S. A. Kates, F. Albericio), Marcel Dekker, New York, **2000**, pp. 79 – 102.

[47] D. Andreu, E. Nicolas, in *Solid-Phase Synthesis* (Eds.: S. A. Kates, F. Albericio), Marcel Dekker, New York, **2000**, pp. 365 – 375.

[48] M. Vila-Perello, A. Sanchez-Vallet, F. Garcia-Olmedo, A. Molina, D. Andreu, *FEBS Lett.* **2003**, *536*, 215 – 219.

[49] R. T. Lee, H. J. Gabius, Y. C. Lee, *Glycoconj. J.* **1998**, *15*, 649 – 655.

[50] P. Guntert, W. Braun, K. Wuthrich, *J. Mol. Biol.* **1991**, *217*, 517 – 530.

[51] S. J. Weiner, P. A. Kollman, D. A. Case, U. C. Singh, C. Ghio, G. Alagona, S. Profeta, P. Weiner, *J. Am. Chem. Soc.* **1984**, *106*, 765 – 784.

[52] D. A. Pearlman, D. A. Case, J. W. Caldwell, W. S. Ross, T. E. Cheatham, S. Debolt, D. Ferguson, G. Seibel, P. Kollman, *Comput. Phys. Commun.* **1995**, *91*, 1 – 41.

[53] A. Germer, C. Mugge, M. G. Peter, A. Rottmann, E. Kleinpeter, *Chem. Eur. J.* **2003**, *9*, 1964 – 1973.

[54] T. Weimar, R. J. Woods, in *NMR Spectroscopy of Glycoconjugates* (Eds.: J. Jiménez-Barbero, T. Peters), Wiley-VCH, Weinheim, **2002**, pp. 111 – 114.

[55] M. G. Ford, T. Weimar, T. Kohli, R. J. Woods, *Proteins* **2003**, *53*, 229 – 240.

[56] C. Sagui, T. A. Darden, *Annu. Rev. Biophys. Biomol. Struct.* **1999**, *28*, 155 – 179.

[57] J. P. Privat, F. Delmotte, G. Mialonier, P. Bouchard, M. Monsigny, *Eur. J. Biochem.* **1974**, *47*, 5 – 14.

[58] R. U. Lemieux, *Acc. Chem. Res.* **1996**, *29*, 373 – 380.

[59] J. P. Carver, *Pure Appl. Chem.* **1993**, *65*, 763 – 770.

[60] J. P. Carver, S. W. Michnik, A. Imberty, D. A. Cumming, *Ciba Foundation Symposia* **1989**, *145*, 6 – 26.

[61] K. A. Kronis, J. P. Carver, *Biochemistry* **1985**, *24*, 834 – 840.

[62] A. C. Muntau, A. A. Roscher, W. H. Kunau, G. Dodt, *Adv. Exp. Med. Biol.* **2003**, *544*, 221 – 224.

[63] C. S. Wright, *J. Biol. Chem.* **1992**, *267*, 14345 – 14352.

[64] H. C. Siebert, S. Andre, J. L. Asensio, F. J. Canada, X. Dong, J. F. Espinosa, M. Frank, M. Gilleron, H. Kaltner, T. Kozar, N. V. Bovin, C. W. von der Lieth, J. F. Vliegenthart, J. Jimenez-Barbero, H. J. Gabius, *ChemBioChem* **2000**, *1*, 181 – 195.

[65] G. L. Ellman, *Arch. Biochem. Biophys.* **1958**, *74*, 443 – 450.

[66] A. Bax, D. G. Davis, *J. Magn. Reson.* **1985**, *65*, 355 – 360.

[67] A. Kumar, R. R. Ernst, K. Wuthrich, *Biochem. Biophys. Res. Commun.* **1980**, *95*, 1 – 6.

[68] P. Guntert, C. Mumenthaler, K. Wuthrich, *J. Mol. Biol.* **1997**, *273*, 283 – 298.

[69] R. M. Scheek, W. F. van Gunsteren, R. Kaptein, *Methods Enzymol.* **1989**, *177*, 204 – 218.

[70] S. C. Gill, P. H. von Hippel, *Anal. Biochem.* **1989**, *182*, 319 – 326.